PHYSICAL REVIEW MATERIALS **8**, 064003 (2024)

Theory of mechanical exfoliation of van der Waals bonded layered materials

Haoye Sun,[1] Ozan Sahin,[1] Ali Javey,[2,3] Joel W. Ager,[1,3] and D. C. Chrzan[1,3]
[1]*Department of Materials Science and Engineering, University of California, Berkeley, California 94720, USA*
[2]*Department of Electrical Engineering and Computer Sciences, University of California, Berkeley, California 94720, USA*
[3]*Materials Sciences Division, Lawrence Berkeley National Laboratory, Berkeley, California 94720, USA*

(Received 14 September 2023; accepted 31 May 2024; published 20 June 2024)

A theoretical framework for analyzing the mechanical exfoliation of 2D materials at finite temperature is introduced. As an example, this framework, based on transition-state theory and calculation of the reaction pathway, is applied to the mechanical exfoliation of multilayer $\mathrm{MoS_2}$. The theory predicts that altering the bonding of the top layer to the bulk through straining or twisting and slowly exfoliating at low temperatures will enhance the yield of the monolayer material.

DOI: 10.1103/PhysRevMaterials.8.064003

I. INTRODUCTION

van der Waals bonded layered materials and their monolayer forms are of great interest for electronic and optoelectronic applications [1–5]. Such materials have strong intralayer covalent bonds, but weak bonding between the layers, generally 10^2–10^3 times weaker [6,7]. As a consequence, monolayers can be separated from the bulk using a mechanical exfoliation approach [8]. Remarkably, tape-mediated mechanical exfoliation and transfer is one of the most successful techniques to obtain "high-quality" 2D monolayers while retaining their intrinsic properties [9]. However, mechanical exfoliation is typically not thought of as a viable method for large-scale manufacture of 2D monolayers because of its low yield, small produced sample sizes, lack of controlled placement of the samples, and the need for a variable number of repeated exfoliation steps.

Recently, it has been shown that a one-step exfoliation process employing a sacrificial metal film can reliably produce and place monolayer samples with linear dimensions of the order of 100 μm with yields approaching 50% [10–14]. Increasing this yield to near 100% will require a deep understanding of the exfoliation process and the factors that limit the yield.

In this paper, we propose a framework for analyzing and optimizing the relevant parameters that influence the yield in the exfoliation process. This framework enables us to examine how temperature and exfoliation velocity affect the final exfoliation results and to understand the mechanisms underlying thermally activated exfoliation processes. We initiate our analysis by simulating the mechanical exfoliation and adhesion processes at zero temperature, at both the atomic and rigid layer levels. In both levels' simulations, we have found a critical stretching displacement beyond which metastable states-precursors to exfoliation occur. Beyond this displacement, a thermally activated transition can take place from the bulk sample to different exfoliation morphologies, each defined by the number of exfoliated layers. These transitions are modeled as competing Poisson processes, with rates estimated using classical transition-state theory. Our numerical calculations suggest that the probability distribution of each exfoliation morphology is significantly influenced by both temperature and strain rate. Additionally, our results indicate that altering the bonding of the top layer to the remaining layers by either straining or twisting the topmost monolayer increases the monolayer selectivity. The subsequent sections detail the implementation of our framework for estimating the yield of monolayers.

II. MECHANICAL EXFOLIATION AND READHESION PROCESS

A. Rigid layer model and potential

The mechanical exfoliation process is first considered with the rigid layer model and then compared with limited calculations on the atomic scale. In this rigid layer model, we assume that the very low-frequency phonon modes, in which the layers move as rigid units, govern the stability of the system [6,7]. Accordingly, we assume that the system consists of a finite number of rigid atomic layers bound to one another via van der Waals (vdW) bonds. The vdW interaction energy between two layers is approximated by summing over pairwise Lennard-Jones (LJ) potential of all pairs of atoms belonging to the different layers,

$$E_{\text{bilayer}} = \sum_i \sum_j V_{LJ}(r_{ij}), \tag{1}$$

with

$$V_{LJ}(r_{ij}) = 4\varepsilon_{ij}\left[\left(\frac{\sigma_{ij}}{r_{ij}}\right)^{12} - \left(\frac{\sigma_{ij}}{r_{ij}}\right)^{6}\right]. \tag{2}$$

Here, i runs over atoms from one of the layers and j runs over atoms from the other layer. V_{LJ} is the parametrized LJ 12-6 potential. This sum is not performed analytically. Instead, the interaction energy between two planes is computed numerically at different separation distances. The data is tabulated and an interpolation function (cubic spline) is made to describe the interlayer interaction energy. For a system consisting of N layers, the total energy is taken as sum over

TABLE I. The parameters that arise from the fitting of the interlayer potential in the form of the Mie potential. AA-twisted 2.87° and AB-twisted 2.87° are found to have the same set of fitted parameters, as they have the same coincident site lattice. (See Appendix.)

Pair	$\varepsilon_{p,q}$	$\sigma_{p,q}$	$m_{p,q}$	$n_{p,q}$
AA	0.0153919	6.08426	29.2657	5.95069
AB	0.0282636	5.61005	19.1211	6.3374
A-twisted 2.87°	0.0211172	5.83632	26.1227	5.69559

all interlayer interaction energies,

$$E_{\text{total}} = \frac{1}{2}\sum_{p=1}^{N}\sum_{q=1}^{N}(1-\delta_{pq})E_{p,q}(d_{pq}) \tag{3}$$

with δ_{pq} the Kronecker δ function, and $E_{p,q}(d_{pq})$ the bilayer interaction energy between layers p and q separated by a distance d_{pq}.

Empirically, it is observed that the resulting interactions can be modeled using a Mie potential [15],

$$E_{p,q}(d) = \varepsilon_{p,q}\left[\left(\frac{\sigma_{p,q}}{d}\right)^{m_{p,q}} - \left(\frac{\sigma_{p,q}}{d}\right)^{n_{p,q}}\right]. \tag{4}$$

In this scheme, the tabulated data is fitted to the Mie potential form with fitting parameters: $\varepsilon_{p,q}$, $\sigma_{p,q}$, $m_{p,q}$, $n_{p,q}$. In this study, the multilayer MoS_2 system is chosen as a prototype and the parametrized LJ 12-6 potential for the Mo-S system is used [16,17]. The parameters resulting from the fitting are shown in Table I. A comparison of the interpolation function and the Mie-type layer pair potentials for different stackings is shown in Fig. 1. For the system studied below, the total energy is calculated as the sum of all Mie-type layer pair potentials. This formulation of energy is then employed to investigate the mechanical exfoliation process and to search for the minimum energy path for thermal activated transition.

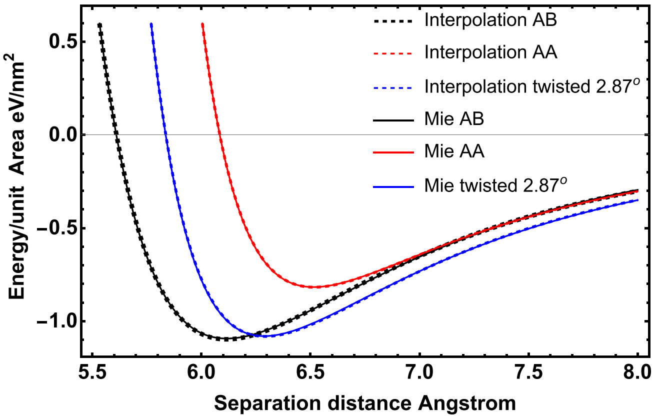

FIG. 1. Bilayer energy per unit area is plotted as a function of interlayer separation for different stackings. Here the interlayer separation for bilayer MoS_2 is defined by Mo-Mo separation. The interpolation function is plotted in dashed lines to compare with the fitted Mie-type potential in solid lines.

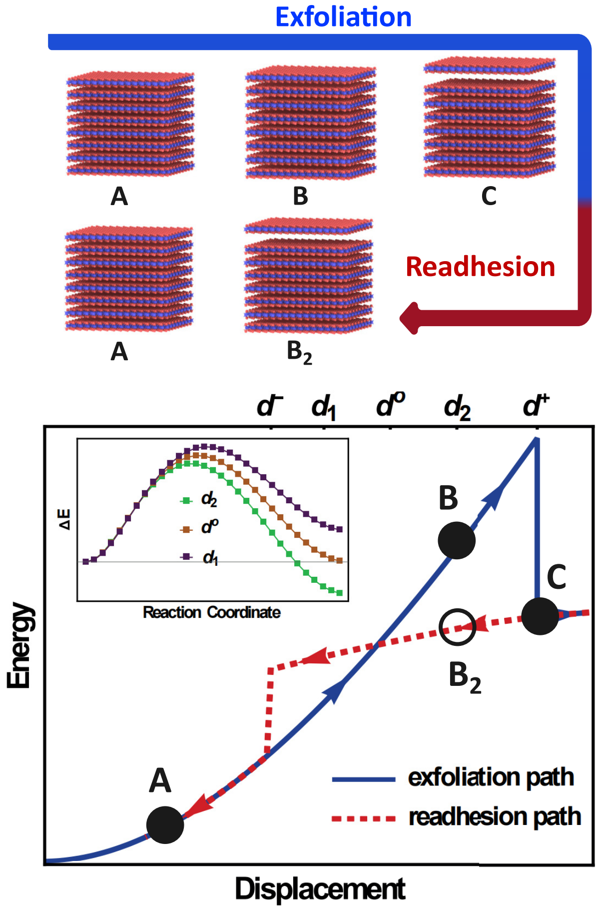

FIG. 2. A sketch of the energy as a function of sample stretch displacement. As the sample is stretched, the energy increases following the blue curve in the figure. If the exfoliated layer(s) are then slowly brought towards the substrate, the energy follows the red curve. For displacements between d^- and d^+ thermally activated transitions between two states are possible. (Inset) Schematic of the minimum energy paths between the two states at the distances d_1, d^o, and d_2.

B. Exfoliation simulation

In the initial state of the exfoliation simulation, the total energy of the multilayer system is minimized using the interior point method to find the equilibrium positions for each monolayer [18,19]. Then the upper and lower layers are pulled apart step by step, stretching the sample along the direction normal to the exfoliated layers. For each stretch displacement (0.05 Åincrements) the positions of all middle layers are adjusted to minimize the internal energy. The energy and minimum energy configuration are recorded, and this process is repeated until the system displays a sharp energy drop, signifying the exfoliation event. Then readhesion simulation is performed using a similar process. The exfoliated layer(s) is(are) then displaced towards the remaining layers with the same step magnitude (0.05 Å). The local minimum energy and associated configuration in this readhesion process are calculated and recorded until the system is restored to its uniformly stretched configuration.

Figure 2 shows schematically the energy paths for exfoliation and readhesion of the topmost layer. Note that this is one

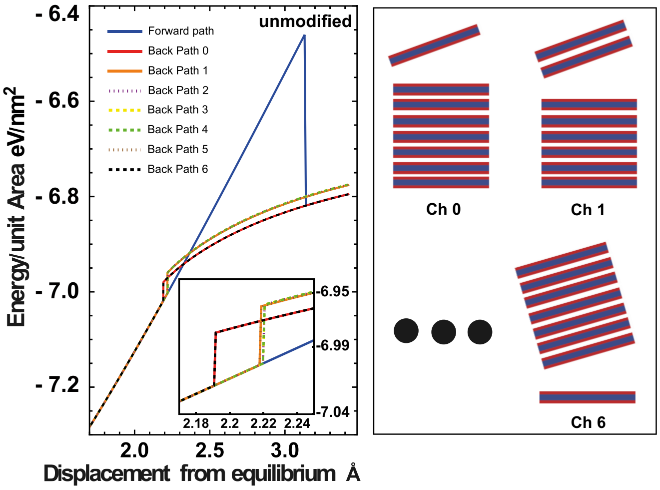

FIG. 3. Energy vs displacement curves for all possible channels in an unmodified eight-layer MoS_2 system. The Backward Path i represents the readhesion process of Channel i. The inset is a closeup view of the readhesion paths. Channel 0 and Channel 6 have equivalent energy due to symmetry of the sample but lead to distinct exfoliation morphologies. The same applies to Channel 1 and Channel 5, as well as Channel 2 and Channel 4.

of the ground-state exfoliation morphologies at zero temperature [20]. At finite temperatures, however, multiple competing morphologies become thermally accessible and therefore need to be considered. Here, we refer to each transition path leading to a particular exfoliation morphology as an exfoliation channel. In an M layer system, there are $M-1$ exfoliation channels: Channel 0 corresponds to the exfoliation of the top layer only, Channel 1 to the exfoliation of the top two layers, continuing to channel $M-2$, which involves the exfoliation of all layers except the bottom one. Taking the eight-layer MoS_2 as an example, all energy pathways associated with different exfoliation morphologies are shown in Fig. 3.

C. Comparison with atomic-level study

The exfoliation process of multilayer MoS_2 has been also studied at atomic level using LAMMPS packages (versions 29Oct2020) [21]. The intralayer atomic interactions of Mo and S atoms are described using reactive empirical bond order potential REBO and the interlayer nonbonded van der Waals (vdW) interactions are described using Lennard-Jones 12-6 potential with extended cutoff (4.5 sigma) [16,17,22]. Each exfoliation simulation is implemented on a sample composed of a fixed number of MoS_2 layers. Periodic boundary conditions are applied in the x and y directions but not in z direction, which is chosen to be the exfoliation direction. Both the upper and lower sulfur layers are considered as rigid entities, a hypothesis grounded in their attachment to either the metallic film (deposited on the top layer) or the substrate, exhibiting higher bending stiffness compared to the middle layers. Exfoliation/readhesion simulations are conducted following the same procedures as in the rigid layer study but using algorithm FIRE and allowing atomic degrees of freedom [23]. The exfoliation path is derived by recording the atomic configurations and energy while stretching the sample to fracture. The readhesion paths are obtained by initiating from varying exfoliation morphologies and gradually returning to a uniformly strained state. The energy vs stretch curves depicted in Fig. 4 display hysteretic features analogous to those observed in the rigid layer study.

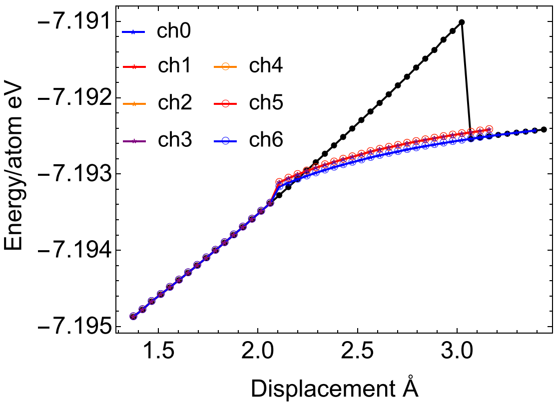

FIG. 4. Atomic scale calculations of energy vs displacement curves for an eight-layer MoS_2 system.

III. MECHANISM UNDERLYING EXFOLIATION PROCESS

A. Zero-temperature and linear stability analysis

Turning to Fig. 2, consider the quasistatic stretching of the stack of presumed rigid layers imposed by fixing the bottom layer and displacing the top layer in the exfoliation direction. The exfoliation/readhesion path displays hysteresis. Within the hysteretic region, there are two (meta)stable states, henceforth referred to a uniformly strained [1] and exfoliated. Up to a displacement d^-, the uniformly strained state is absolutely stable. At displacements between d^- and d^o, the uniformly strained state is the lowest-energy state, but the exfoliated state has become metastable. In this region, a thermally activated transition to the exfoliated state is possible. Between d^o and d^+, the exfoliated state is now the lowest-energy state, and the transition between states remains thermally activated. For displacements greater than d^+, only the exfoliated state is stable while uniformly strained state is mechanically unstable, which can be revealed by a linear stability analysis of the tensile vibrational modes [20].

At zero temperature, when the system is exfoliated adiabatically, it remains trapped in the uniformly strained state until reaching d^+. As displacement approaches this threshold, the frequency of one of the tensile vibrational modes drops to zero. Previous paper [20] argues that at zero temperature the eigenvector of this mode defines the morphology of the exfoliation event.

An example of such analysis for a system of eight layers of MoS_2 is shown in Fig. 5. As can be seen in the figure, all vibration modes soften throughout the exfoliation process. One of the modes reaches zero frequency first (marking the exfoliation event), while the other modes remain stable. How-

---

[1] The state is not truly uniformly strained, as the displacements of the layers vary with the distances to the free surfaces of the film.

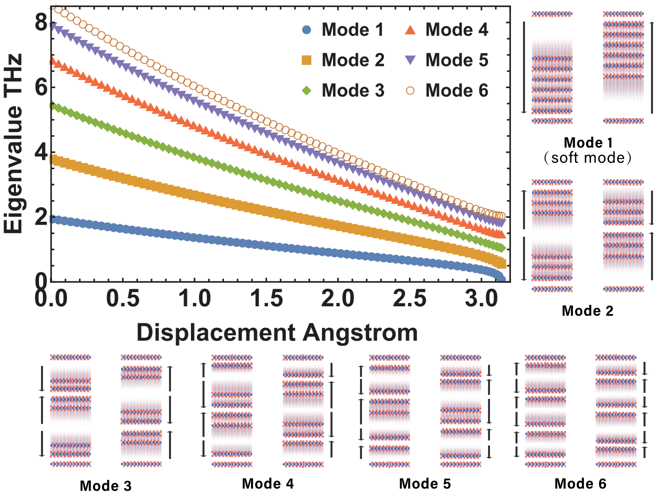

FIG. 5. The calculated frequency for each normal mode as function of exfoliation displacement. The structure with the oscillating displacement vector for all mode are shown. The black arrows indicate the vibration direction for the layers.

ever, consider the stretch displacement step immediately prior to exfoliation. For the mode with vanishing frequency, its associated eigenvector causes maximal interlayer separation (during the course of one period) between the top two layers or equivalently between the bottom two layers. This implies that there is an equal chance of exfoliating either the top layer or all but the bottom layer, which is consistent with the overall symmetry of the problem.

Monolayer selectivity during exfoliation can be enhanced by breaking the symmetry of the eigenvectors of the exfoliation mode and tuning the lowest-frequency eigenmode to the desired exfoliation morphology [20]. Compressively straining the top layer of the stack weakens the bonding of this layer to the stack due to the moiré pattern that forms and enhances the monolayer selectivity of the exfoliation process.

Misorienting the top monolayer of the stack with a twist angle with respect to layers beneath it should introduce a similar moiré pattern, and should also enhance monolayer selectivity. A normal mode analysis of the twisted state (see the Appendix) following the procedure in [20] finds that twisting the top layer of the source should also strongly favor monolayer exfoliation, as shown in Table II. These observations rationalize the effectiveness of the recently developed thin-film-mediated method in monolayer selectivity attributed to straining the top layer of the stack [10–14,24] and suggest that a twist-mediated method should lead to a similar and potentially better improvement in exfoliation monolayer yields.

B. Finite temperature and thermally activated transition

At finite temperature, the exfoliation morphology is not necessarily determined by the softest vibration mode because there are multiple competing exfoliation channels that are thermally accessible simultaneously before the sample reaches mechanical instability. The probability of obtaining a specific exfoliation channel is determined by the relative probabilities of transitions through the competing exfoliation channels.

TABLE II. Normalized eigenvectors and caused interlayer separation changes associated with the lowest-frequency mode for a six-layer MoS_2 system under different conditions: (natural) the top layer is unmodified, (strained) the top layer is 5% compressively strained, and (twisted) the top layer is misoriented with a commensurate angle (2.87°).

Eigenvectors associated with the lowest-frequency mode						
Layer	Layer 1	Layer 2	Layer 3	Layer 4	Layer 5	Layer 6
Natural	0	0.419	0.569	0.569	0.419	0
Strained	0	0.308	0.497	0.587	0.560	0
Twisted	0	0.305	0.483	0.580	0.581	0
Layer-layer separation changes						
Layer	NA	L2-L1	L3-L2	L4-L3	L5-L4	L6-L5
Natural	NA	0.419	0.150	0	0.150	0.419
Strained	NA	0.308	0.189	0.090	0.027	0.560
Twisted	NA	0.305	0.178	0.097	0.001	0.581

Consider a uniformly strained sample that is exfoliated through Channel 0, the top layer exfoliation event. Define the rate at which the system transitions to the exfoliated state n at time t to be $R_n(t)$. Define the probability that the channel exfoliation event 0 has not occurred up to time t to be $q_0(t)$. The probability that the exfoliation event has not happened up to time $t + dt$ is then given by

$$q_0(t + dt) = q_0(t)(1 - R_0(t)dt). \tag{5}$$

Integrating gives an expression for $q_0(t)$,

$$q_0(t) = \exp\left[-\int_0^t dt' R_0(t')\right]. \tag{6}$$

This expression explicitly accounts for the time dependence of the transition rates, arising from the temporal stretching of the sample during the exfoliation process.

Accordingly, the probability that the monolayer exfoliates at time between t and $t + dt$, defined to be $p_0(t)\,dt$, is simply the probability that the monolayer has not exfoliated up to time t multiplied by the exfoliation probability during the time dt,

$$p_0(t)\,dt = R_0(t)\,dt\,\exp\left[-\int_0^t dt' R_0(t')\right]. \tag{7}$$

This expression considers only one channel. When there are competing exfoliation channels, the expression for the probability of obtaining exfoliation channel n at at time between t and $t + dt$ before any other exfoliation event becomes

$$p_n(t)\,dt = R_n(t)\,dt\,\exp\left[-\int_0^t dt' \sum_{n=0}^{N} R_n(t')\right], \tag{8}$$

with $N = M - 2$ the total number of exfoliation channels.

The total probability of obtaining an exfoliation event corresponding to channel n is simply the integral of $p_n(t)$ over all exfoliation times, while the displacement is between d^- (at time $t = 0$) and d^+ (at time $t = t_{\mathrm{end}}$). For example, the probability to obtain Channel 0, defined to be P_0, is

$$P_0 = \int_0^{t_{\mathrm{end}}} d\tau R_0(\tau) \exp\left[-\int_0^{\tau} dt' \sum_{n=0}^{N} R_n(t')\right]. \tag{9}$$

Evaluating Eq. (9) requires a physical model for the transition rates from the uniformly strained to the exfoliated state. As an example application of Eq. (9), it is assumed that the rates can be computed using classical transition-state theory [25,26] combined with the rigid layer model. This approximation facilitates the computation of transition rates as a function of layer separation. This approximation is helpful because the integrals in Eq. (9) must be performed numerically for different thermal energy densities and exfoliation stretch velocities, etc.

C. Classical transition-state theory

In an initial approximation, it is assumed that thermodynamic equilibrium is maintained throughout the system and that once the system crosses the transition barrier, it does not recross. Then the transition rates for different exfoliation channels R_n are dependent on the corresponding energy barriers and can be estimated according to

$$R_n = k_o(n) \exp\left(-\frac{\Delta E(d, n, T, A)}{k_B T}\right). \tag{10}$$

where $k_o(n)$ is the attempt frequency for channel n, k_B is Boltzmann's constant, ΔE is the exfoliation energy barrier, which is dependent on the loading displacement d, the exfoliation channel n, the temperature T, and the sample area A.

In the rigid layer model, the interaction energies between layers of finite area are approximated by the product of the area of the layer A, and the interaction energy per unit area between two infinite sheets,

$$E_{\mathrm{int}}(z, n, T, A) = A\, E^{\infty}(z, n, T = 0), \tag{11}$$

with $E^{\infty}(z, n, T = 0)$ the interaction energy per unit area between two infinite layers separated by a distance z computed at zero temperature. The energy barriers are then calculated using the interaction energy in (11) and the nudged elastic band (NEB) method [27,28]. Note that the calculated energy barriers scale linearly with the area of the film. Consequently, the temperature appears within the model only in the combination $\frac{k_B T}{A}$, and the following will consider the predicted properties of the model to be a function of this thermal energy density.

For the M rigid layer system, there are $N = M - 2$ vibrational degrees of freedom. The attempt frequency $k_o(n)$ can be approximated by the ratio of the product of positive eigenvalues at initial state and the product at saddle-point state (excluding the soft mode) in the minimum energy path [25],

$$k_o(n) = \frac{1}{2\pi} \frac{\prod_{i=1}^{N} \lambda_i^{\mathrm{initial}}(n)}{\prod_{i=2}^{N} \lambda_i^{\mathrm{saddle}}(n)}, \tag{12}$$

where the normal-mode eigenvalues $\lambda_i^{\mathrm{initial}}(n) > 0$ for $i = 1...N$, and $\lambda_1^{\mathrm{saddle}}(n) < 0$; $\lambda_i^{\mathrm{saddle}}(n) > 0$ for $i = 2...N$.

D. Nudged elastic band method

The nudged elastic band (NEB) method has been used to determine the minimum energy path (MEP) of the exfoliation event from a stretched state to an exfoliated state in the displacement range between d^- and d^+ [28]. At each displacement step, the initial configuration is chosen from the stretched sample in the exfoliation path, while the final configuration is chosen from the exfoliated state in the readhesion path at the same displacement. A single MEP is computed using 60 replicas (intermediate states) constructed by linear interpolation between the two chosen configurations. The adjacent replicas are connected by a spring with a spring constant equal to 0.0005 eV/Å. The force on each replica contains the parallel component of the spring force and the perpendicular component of the potential force,

$$\begin{aligned} \boldsymbol{F}_i^r &= -(\nabla U_{at}(\boldsymbol{R}_i) - \nabla U_{at}(\boldsymbol{R}_i) \cdot \boldsymbol{\tau}_i), \\ \boldsymbol{F}_i^s &= k_{\mathrm{spring}}(|\boldsymbol{R}_{i+1} - \boldsymbol{R}_i| - |\boldsymbol{R}_i - \boldsymbol{R}_{i-1}|)\boldsymbol{\tau}_i. \end{aligned} \tag{13}$$

The steepest descent algorithm is used to minimize the forces in (13) in order to find the MEP. The calculation is considered converged if the maximum force component in each replica is less than 0.001 eV/Å. The saddle-point configuration (transition state) is taken to be the replica with maximum energy along the MEP. For each channel, the energy barrier is calculated from the energy difference between the initial configuration and the saddle-point configuration. The attempt frequency is calculated using the vibrational eigenfrequencies of the initial configuration and the saddle-point configuration. Examples of MEPs for an unmodified eight-layer sample stretched at representative displacements d_1 and d_2 are shown in Fig. 6.

IV. RESULTS

The computed energy barriers are shown for an eight-layer MoS_2 sample in Fig. 7(a). The energy barriers decrease as the sample stretch increases. Applying a twist to the top layer breaks the symmetry of the problem, reduces the width of the hysteretic region, and yields the lowest-energy barrier for the desired channel, Channel 0. Figure 8 displays the computed attempt frequencies for an unmodified eight-layer MoS_2 sample. The attempt frequencies generally increase with the stretching of the sample. To minimize the noise from the saddle-point frequency calculations, we employed linear regression functions to model the attempt frequencies as functions of displacement. These linear models are then used in our probability calculations.

In applying Eq. (9), it is insightful to consider some limiting forms for the stretch velocity. First, consider that the stretch rate during exfoliation is infinitesimally slow. Empirically, it is observed that not all exfoliation channels become accessible at the same stretch displacement, as shown in Fig. 3. The first mode to soften (Fig. 5) correlates with the first exfoliated state(s) to become metastable. Since return transitions are not included in the theory, the system will transition through this channel because the infinitesimal displacement velocity allows for an effectively infinite time over which only one exfoliation channel is possible. In this case, the final result is consistent with zero-temperature analysis.

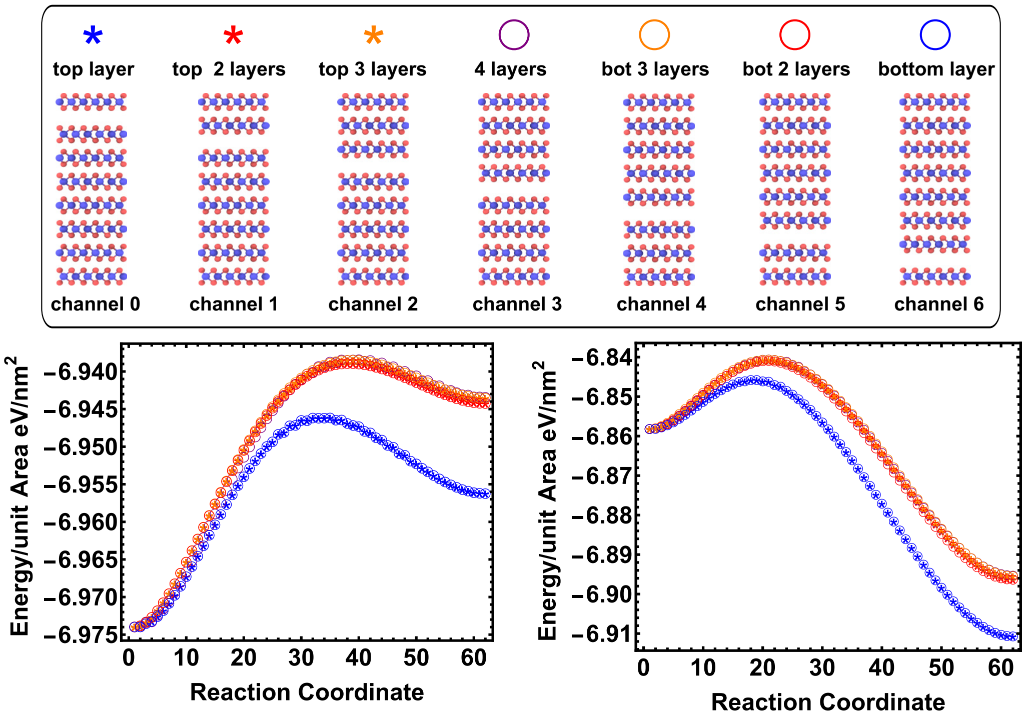

FIG. 6. Minimum energy paths along different exfoliation channels in a unmodified eight-layer MoS_2 at displacement d_1 (left) and d_2 (right).

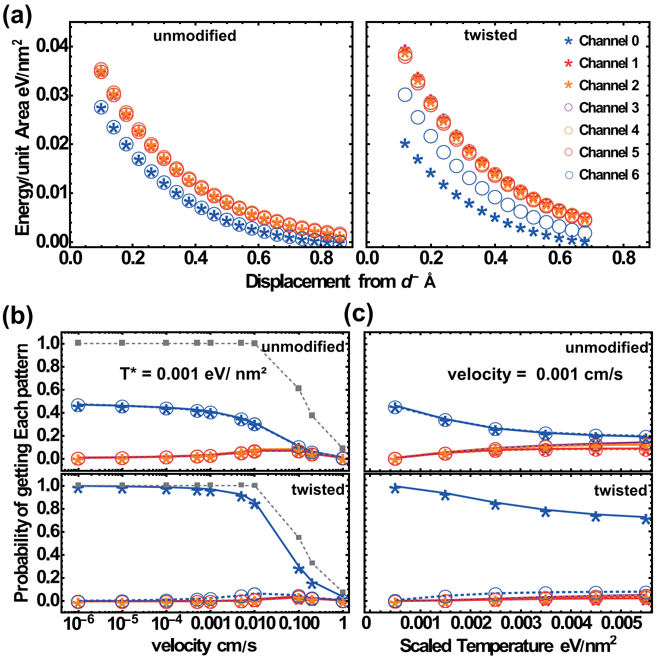

FIG. 7. (a) Displacement-dependent energy barrier for each exfoliation channel is shown for a eight-layer MoS_2. The displacements range from d^- to d^+. (b) Probability of getting each exfoliation state as a function of the assumed constant exfoliation velocity at fixed thermal energy density $\frac{k_BT}{A} = 0.001\ \mathrm{eV/nm}^2$. The gray-dashed line is the sum of the probabilities of all possible outcomes. When, the sum is less than 1, thermally activated exfoliation may not occur up to displacement d^+. (c) Probability of obtaining each exfoliation channel as a function of strain rate at $\frac{k_BT}{A}$ for a fixed velocity of 0.001 cm/s.

A second interesting case is when the sample is stretched instantaneously to a displacement between d^o and d^+, and kept there for all time until exfoliation occurs. In this instance, the rate of exfoliating through the Channel n becomes time independent and Eq. (9) can be integrated to find

$$P_n(T) = \frac{R_n(T,A)}{\sum_{j=0}^{N} R_j(T,A)}, \tag{14}$$

with $R_n(T,A)$ corresponding to the computed values of the rates for the various channels at the fixed displacement.

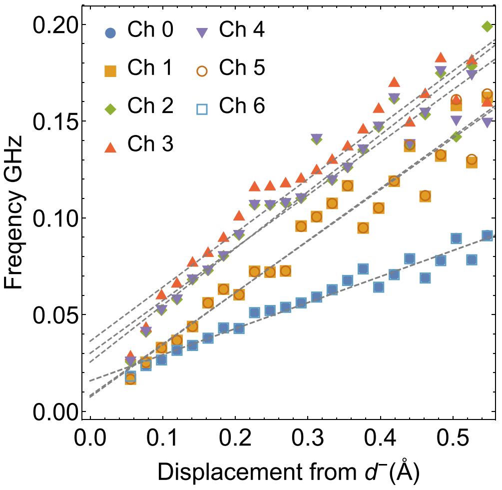

FIG. 8. Attempt frequency for each exfoliation channel in an unmodified eight-layer MoS_2 sample. The gray-dashed lines represent linear regression lines illustrating the trend.

More generally, both the temperature and the exfoliation velocity can be varied experimentally. Predictions based on the assumption of a constant exfoliation stretch velocity are shown in Figs. 7(b) and 7(c).

Figure 7(b) shows that tuning the exfoliation velocity (assumed constant), when coupled with the twisting (or presumably, straining) of the layer to be exfoliated, can increase the probability of exfoliating a monolayer to 1. Specifically, at a thermal energy density of 0.001 $\mathrm{eV/nm^2}$, for velocities below $10^{-4}\mathrm{cms^{-1}}$, the probability of exfoliating a single-twisted layer saturates effectively at 1. The probability, however, begins to roll off at velocity around $10^{-2}\mathrm{cms^{-1}}$ as the probabilities of exfoliating through the other channels increase.

At very high velocities it is possible to span the range of displacements d^- to d^+ before any thermally driven exfoliation event is observed. As shown in Fig. 7(b), the sum of probabilities of all possible exfoliation outcomes is less than 1 when the velocity is greater than 0.01 cm $\mathrm{s^{-1}}$. The model is not applicable in this high-velocity regime. However, intuition suggests that in this regime, the selected exfoliation channel will be random.

Figure 7(c) shows the effects of thermal energy density on the probability of exfoliation given a fixed exfoliation velocity of 0.001 cm $\mathrm{s^{-1}}$. Here, too, there is a definite advantage to twisting the top layer of the sample. In general, increasing the temperature decreases the probability of obtaining the morphology associated with Channel 0.

Taken together, the results presented in Fig. 7 indicate that for the rigid layer model, low exfoliation velocities at low temperatures applied in conjunction with a slight twist will lead to the highest yields of monolayer samples.

V. DISCUSSION

A. Thickness effect

The results of the limiting case represented by Eq. (14) suggest that the number of layers in the stack can also affect the yield. This paper has primarily examined the mechanical exfoliation of an eight-layer sample. This behavior is believed to be similar to that for samples with larger numbers of layers, although the details will be different.

However, there are some subtleties to consider. At first blush, one imagines that increasing the number of layers will increase the number of available exfoliation channels, and thereby decrease the probability of each individual event. This is generally true, but depends on the details of the transition rates. Also, we found our model used for finite temperature is not applicable to samples composed of small number of layers.

Consider the most simple case: A sample consisting of only three monolayers. Stretch the sample by holding the top monolayer and bottom monolayer at fixed positions separated by an amount d, and then vary the position of the middle layer. The resulting energy profiles are plotted for different d in Fig. 10. At low stretches, the energy vs position curve displays a single minimum, indicating that only the "uniformly" strained state is stable. For d greater than a critical stretch, approximately $d = 13.2$ Å, this minimum becomes a local maximum and two minima emerge. This bifurcation point coincides with the exfoliation event. There is no hysteretic region in the exfoliation and readhesion path because the uniformly strained and exfoliated states cannot coexist.

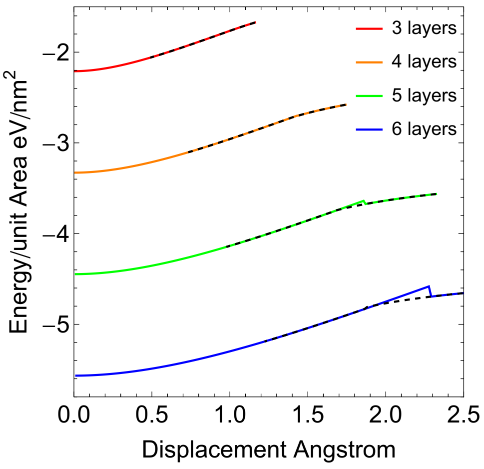

FIG. 9. Energy per unit area is plotted as a function of displacement for few layer samples.

For samples with four or more layers, the analysis becomes very similar to that of the eight-layer system. A hysteretic region can be identified and energy barriers computed. However, the range of the hysteretic region can be quite small.

For example, consider the behavior of the four-layer system (without rotating that top layer). For $d < 19.7125$ Å, only the uniformly stretched state is stable. For $19.7125\ \text{Å} \leqslant d \leqslant 19.7422$ Å, the two symmetrically equivalent single-layer exfoliated states coexist with the uniformly stretched state. For $d > 19.7422$ Å, the uniformly stretched state is no longer stable but instead replaced with the state in which two layers are exfoliated. Thus, while this system looks promising for obtaining single-layer exfoliation, the extremely small differences in displacements defining the hysteretic region make it unlikely that this approach will be useful experimentally and call into question the use of simple transition-state theory.

Increasing the number of layers in the sample increases the span of the hysteretic region. The results for 4–6 layer systems are shown in Fig. 9.

B. Limitation of rigid layer model

It is noted that the rigid layer model is not a perfect description of exfoliation physics. As the sample area increases and the layers are allowed to bend, it is more likely that the energy barrier to the exfoliated state will be determined by the formation of a critical-sized penny crack in the sample. For samples below a critical nucleus size, the rigid-layer model is appropriate. Similar to other nucleation problems, if the driving force is smaller (in this case the driving force increases with displacement), the critical nucleus size is expected to be larger. Therefore, if exfoliation occurs early in the process, the rigid layer model may be applicable. As the displacement increases, the details of the rates will change. We need to integrate atomic-level studies of the transition path with our proposed framework to enhance the precision of final yield predictions. The atomic scale calculation of transition pathways allows an improved estimation of energy

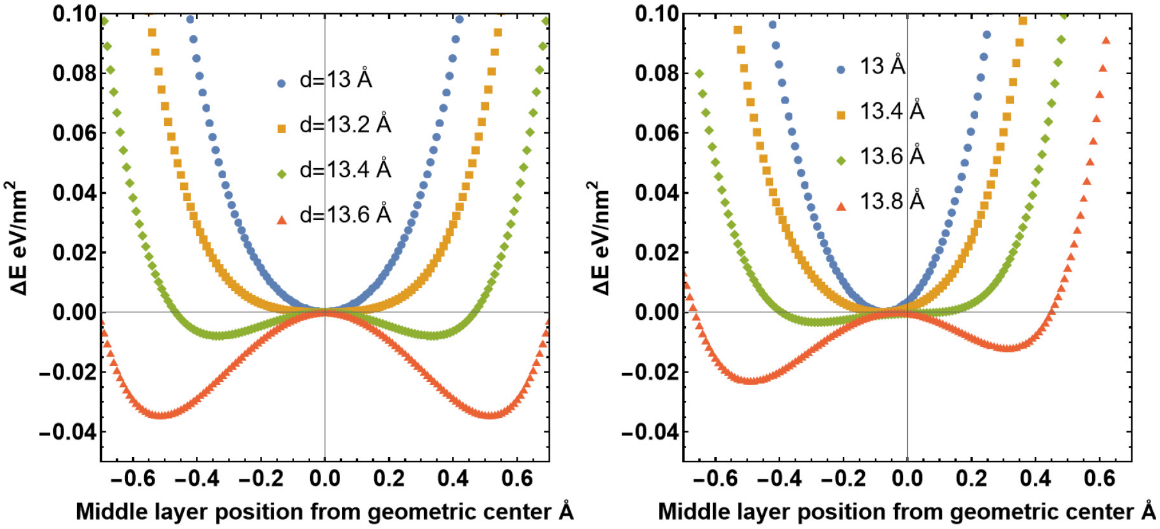

FIG. 10. Plots of the energy as a function of the position of the middle layer for various values of d for (left) natural sample and (right) sample with a twisted top layer.

barriers and attempt frequencies within the hysteretic regions. As a demonstration, we compute the energy barrier using a quasi-one-dimensional system made up of eight-layer MoS_2. Full periodicity is imposed in the plane of the sample. The supercell is chosen to mimic the properties of nanoribbons with one direction fixed to be a short distance, while the other distance is variable. The short period in one direction of the unit cell makes the cell effectively rigid in that direction, so that bending only in one direction is possible. By varying the length of the long side of the supercell, we can compute the energy barrier as a function of the sample size.

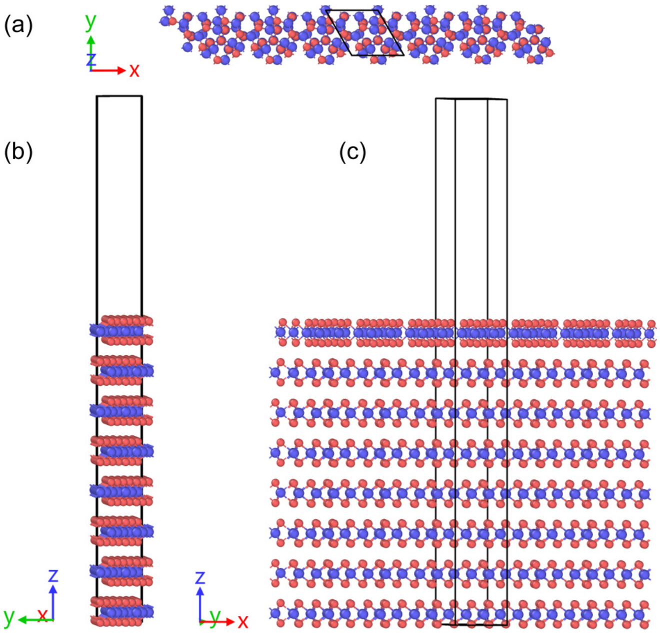

FIG. 11. The structure of quasi-one-dimensional supercell for the sample with the top layer twisted by 38.21°. The primitive unit cell is indicated by the black box. (a) Top view, (b) side view, and (c) front view.

To show the effect of twist, we consider a sample in which the top layer is twisted by 38.21°. This rotation angle is chosen because of its near match with the cell size of the unmodified sample. Figure 11 presents the primitive unit cell and supercell for the twisted sample, where the primitive unit cell contains 56 Mo atoms and 112 S atoms (eight monolayers). The supercell is constructed by fixing the dimension y (width) to be one unit cell, and we increase the number of unit cells in the x direction (length).

Using the LAMMPS code, exfoliation/readhesion simulations are performed for each sampled size. We take a single point in the hysteric region as an example, specifically when both the unmodified sample and the twisted sample are stretched by 2.5 Å from their respective equilibrium structures. The initial configuration corresponds to a uniformly strained state, while the final configurations correspond to the exfoliated states. Sixteen replicas are constructed by linear interpolation between initial and final configurations, with adjacent replicas connected by a spring constant equal to 0.0005 eV/Å. We employ the NEB method implemented in the LAMMPS code [27,28] in conjunction with the FIRE algorithm, setting the convergence criterion for the two-norm force to 0.002 eV/Å, to calculate the energy barriers and corresponding minimum energy paths.

Our results, depicted in Fig. 12, indicate that the energy barrier for exfoliation reaches a threshold associated with the nucleation energy of crack formation. Note that the energy barrier for this chosen displacement converges at a system length of approximately 10 nm. Smaller initial displacements will require larger systems to converge the energy barrier for exfoliation.

The predictions for the energy barrier at the chosen displacement align qualitatively with the predictions from the rigid layer model. Specifically, introducing a rotation to the top monolayer substantially reduces the energy barrier for exfoliation, thereby enhancing selectivity for monolayer exfoliation. The behavior of a sample large enough to bend in both directions is likely to be similar to that presented for both

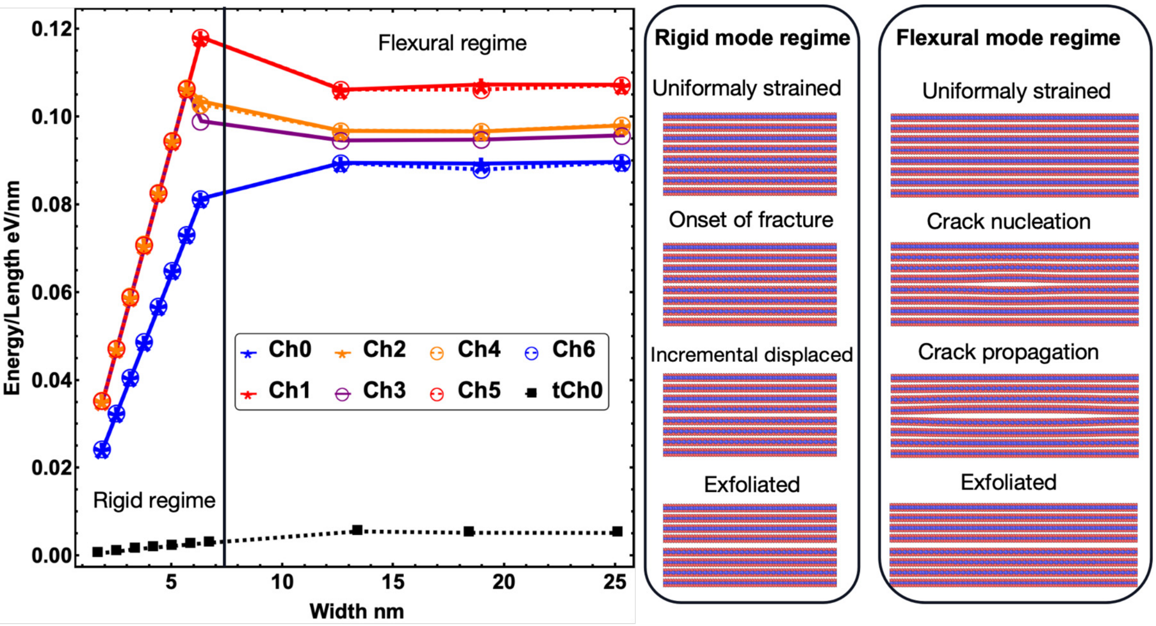

FIG. 12. Energy barriers for an eight-layer MoS_2 system both with an unmodified top monolayer (Ch0–6) and with a top monolayer twisted by 38.21° (tCh0), are calculated at a stretch displacement magnitude of 2.5 Åfrom their equilibrium structures. The atomic configurations in the minimum energy path for Channel 3 of the unmodified sample are displayed on the right side. For small-scale samples, where layers behave as rigid units, the energy barrier scales proportionally with sample size. However, beyond a certain size threshold, the energy barrier is dictated by the nucleation energy of crack formation. Remarkably, in both size regimes, energy barriers are substantially diminished in the presence of a twist in the samples.

the rigid layer model and the 1D penny crack model. Detailed analysis of this case is left to future work.

VI. CONCLUSIONS

The ability to mechanically exfoliate large monolayer samples of 2D materials in one (or controlled number of) step is highly desired for both research and commercial applications. In this paper, a theoretical framework for analyzing the effects of temperature and exfoliation velocity on yield is developed. The model is solved within the context of the rigid layer model. This model predicts that growing a sacrificial metal film on the top layer that strains and/or is used to twist the top layer will increase the probability of exfoliating a monolayer. This probability will also increase if the sample is slowly exfoliated at low temperatures.

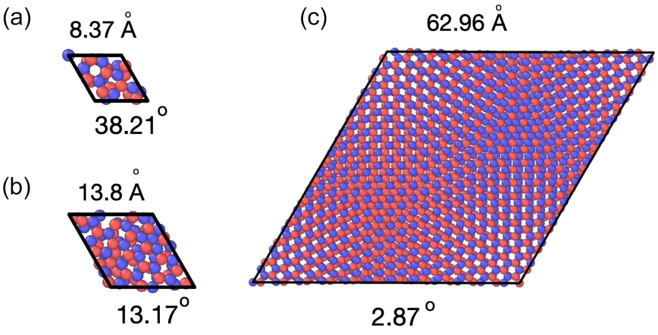

FIG. 13. Top views of the coincidence lattice of bilayer MoS_2 with misorentation angle (a) 38.21°, (b) 13.17°, and (c) 2.87°.

ACKNOWLEDGMENTS

This work was supported by the U.S. Department of Energy, Office of Science, Office of Basic Energy Sciences, Materials Sciences and Engineering Division under Contract No. DE-AC02-05Ch11231 (Electronic Materials program).

APPENDIX

Twisted-bilayer and multilayer structure

The twisted-bilayer MoS_2 system is obtained by stacking one rotated monolayer of MoS_2 on top of a sample with bulk

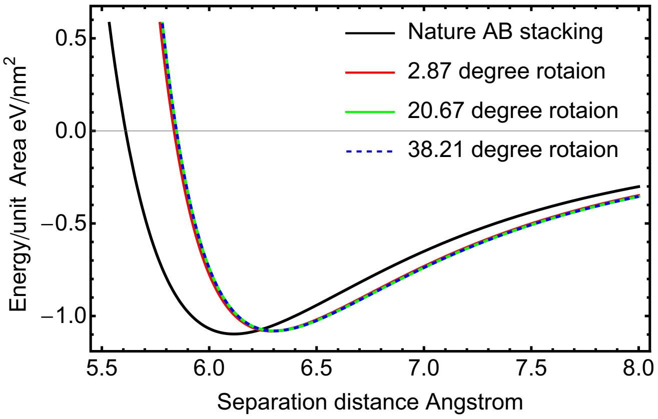

FIG. 14. Interlayer potential energy as a function of separation with different top layer conditions: (1) top layer is unmodified, (2) the top layer is twisted 2.87°, (3) the top layer is twisted 20.67°, and (4) the top layer is twisted 38.21°.

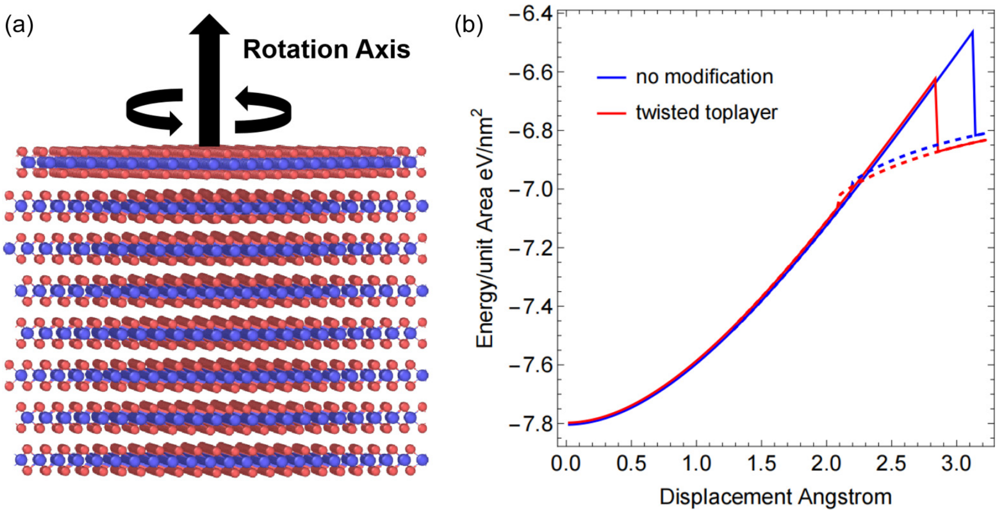

FIG. 15. (a) A schematic of how to construct the twisted eight-layer structure. (b) Energy per unit area is plotted as a function of a eight-layer sample stretch displacement, which is compared to a twisted eight-layer sample.

stacking. The rotation angle θ is chosen to be one of the special angles that ensures that the overall structure remains periodic within the plane of the layer. The corresponding commensurate supercell is defined by pairs of lattice sites that match exactly under rotation, the so-called coincident site lattice (CSL).

Finding the CSL is equivalent to finding the reciprocal of the displacement shift lattice (DSL) of their reciprocals [29–31]. Define $\mathbf{E}$ to be the generating matrix of the first-plane lattice and $\mathbf{RE}$ to be the generating matrix of the rotated plane lattice, with $\mathbf{R}$ being the corresponding rotational matrix. The respective reciprocal lattices are defined as $\mathbf{E}^{-T}$ and $\mathbf{RE}^{-T}$, respectively. Then the displacement shift lattice (DSL) of these two reciprocal lattices can be constructed by a 3 x 6 matrix $[\mathbf{E}^{-T}, \mathbf{RE}^{-T}]$. The primitive lattice vectors of this lattice are found using the Lenstra-Lenstra-Lovász (LLL) lattice basis reduction algorithm [32]. Taking a reciprocal of the resulting reduced generating matrix gives the generating matrix for the CSL. Three example supercells with misorientation angles of 13.17°, 6°, and 2.87°, generated with this method are shown in Fig. 13. Performing the calculation of interlayer interaction energy in (2) for a variety of angles: 2.876°, 4.96°, 6°, 13.17°, 20.67°, and 38.21°. These bilayer systems have nearly the same interlayer energies density if each monolayer is forced to be rigid. This suggests that the interlayer interaction modeled with the LJ potential is insensitive to rotation angle changes. The results for 2.876°, 20.67°, and 38.21° are shown in Fig. 14.

A schematic for an eight-layer sample is shown in Fig. 15(a). A comparison of the exfoliation and readhesion process for Channel 0 this sample and an untwisted sample is shown in Fig. 15(b). The twisted sample shifts the hysteresis region towards smaller displacements.

---

[1] K. S. Novoselov, V. I. Fal'Ko, L. Colombo, P. R. Gellert, M. G. Schwab, and K. Kim, Nature (London) **490**, 192 (2012).
[2] A. K. Geim and I. V. Grigorieva, Nature (London) **499**, 419 (2013).
[3] A. K. Geim, Science **324**, 1530 (2009).
[4] S. B. Desai, S. R. Madhvapathy, A. B. Sachid, J. P. Llinas, Q. Wang, G. H. H. Ahn, G. Pitner, M. J. Kim, J. Bokor, C. Hu *et al.*, Science **354**, 99 (2016).
[5] S. Deng and V. Berry, Mater. Today **19**, 197 (2016).
[6] R. Zallen and M. Slade, Phys. Rev. B **9**, 1627 (1974).
[7] J. N. Israelachvili, in *Intermolecular and Surface Forces*, 3rd ed., edited by J. N. Israelachvili (Elsevier, Amsterdam, 2011), pp. 107–132.
[8] K. S. Novoselov, D. Jiang, F. Schedin, T. J. Booth, V. V. Khotkevich, S. V. Morozov, and A. K. Geim, Proc. Natl. Acad. Sci. USA **102**, 10451 (2005).
[9] M. Yi and Z. Shen, J. Mater. Chem. A **3**, 11700 (2015).
[10] S. B. Desai, S. R. Madhvapathy, M. Amani, D. Kiriya, M. Hettick, M. Tosun, Y. Zhou, M. Dubey, J. W. Ager, D. Chrzan *et al.*, Adv. Mater. **28**, 4053 (2016).
[11] H. M. Gramling, C. M. Towle, S. B. Desai, H. Sun, E. C. Lewis, V. D. Nguyen, J. W. Ager, D. Chrzan, E. M. Yeatman, A. Javey *et al.*, ACS Appl. Electron. Mater. **1**, 407 (2019).
[12] M. Velický, G. E. Donnelly, W. R. Hendren, S. McFarland, D. Scullion, W. J. DeBenedetti, G. C. Correa, Y. Han, A. J. Wain, M. A. Hines *et al.*, ACS Nano **12**, 10463 (2018).
[13] V. Nguyen, H. Gramling, C. Towle, W. Li, D. H. Lien, H. Kim, D. C. Chrzan, A. Javey, K. Xu, J. Ager *et al.*, J. Micro Nano-Manuf. **7**, 041006 (2019).
[14] J. Kim, H. Park, J. B. Hannon, S. W. Bedell, K. Fogel, D. K. Sadana, and C. Dimitrakopoulos, Science **342**, 833 (2013).
[15] G. Mie, Ann. Phys. (Leipzig) **316**, 657 (1903).
[16] T. Liang, S. R. Phillpot, and S. B. Sinnott, Phys. Rev. B **79**, 245110 (2009).

[17] T. Liang, S. R. Phillpot, and S. B. Sinnott, Phys. Rev. B **85**, 199903 (2012).

[18] A. Forsgren, P. Gill, and M. Wright, *Interior Methods for Nonlinear Optimization*, Vol. 44 (SIAM, Philadelphia, 2002).

[19] J. Nocedal and S. J. Wright, *Numerical Optimization* (Springer, New York, 2006).

[20] H. Sun, E. W. Sirott, J. Mastandrea, H. M. Gramling, Y. Zhou, M. Poschmann, H. K. Taylor, J. W. Ager, and D. C. Chrzan, Phys. Rev. Mater. **2**, 094004 (2018).

[21] S. Plimpton, J. Comput. Phys. **117**, 1 (1995).

[22] J. A. Stewart and D. E. Spearot, Modelling Simul. Mater. Sci. Eng. **21**, 045003 (2013).

[23] E. Bitzek, P. Koskinen, F. Gähler, M. Moseler, and P. Gumbsch, Phys. Rev. Lett. **97**, 170201 (2006).

[24] Y. Zhou, D. Kiriya, E. E. Haller, J. W. Ager, A. Javey, and D. C. Chrzan, Phys. Rev. B **93**, 054106 (2016).

[25] P. Hänggi, P. Talkner, and M. Borkovec, Rev. Mod. Phys. **62**, 251 (1990).

[26] G. H. Vineyard, J. Phys. Chem. Solids **3**, 121 (1957).

[27] G. Henkelman and H. Jónsson, J. Chem. Phys. **113**, 9978 (2000).

[28] G. Henkelman, B. P. Uberuaga, and H. Jónsson, J. Chem. Phys. **113**, 9901 (2000).

[29] M. J. Buerger, Z. Kristallogr. **109**, 42 (1957).

[30] H. Grimmer, Scr. Metall. **8**, 1221 (1974).

[31] E. A. Lord, Z. Kristallogr. **221**, 705 (2006).

[32] A. K. Lenstra, H. W. Lenstra, and L. Lovász, Math. Ann. **261**, 515 (1982).